UNIVERSITY OF WEST BOHEMIA

Applied and Computational Mechanics 1 (2007) 489 - 498

Applied and Computational Mechanics

Modelling of railway vehicle movement considering non-ideal geometry of wheels and rails

R. Jandora[a,*]

[a] *Faculty of Mechanical Engineering, Brno University of Technology, Technická 2896/2, 616 69 Brno, Czech Republic*

Received 7 September 2007; received in revised form 8 October 2007

Abstract

A model of railway vehicle movement is presented. This model takes into account arbitrary shape of wheel and rails. Therefore models of contact of surfaces of arbitrary geometry are built in. The contact forces are found with possibility of choice from methods of rolling contact mechanics. The shape irregularities cause vibrations, therefore a model of track and its rails, sleepers and ballast is incorporated and also the vehicle model includes vibration-damping elements. Overall it makes a complete model of the vehicle movement with focus on the wear prediction and vibrations due to the corrugation.

Keywords: wheel-rail contact, train-track interaction, rail corrugation

1. Introduction

Problem of modelling of railway vehicle motion is very common in engineering practice (large projects such as the DFG priority programme System Dynamics and Long-term Behaviour of Vehicle, Track and Subgrade in Germany, work of the State Key Laboratory of Traction Power in China). It helps predict many difficulties that can occur during the vehicle service, e.g. derailment prevention, wear prediction and estimation of vibrations and noise.
Two models focused on effects and prediction of corrugation were presented in literature in past years. The model created by Andersson [1] uses the FASTSIM algorithm (presented in [8]) to calculate the contact forces. The model created by Jin [7] uses the formulas by Shen, Hedrick and Elkins presented in [8]. It was shown in the previous work of the author [5] that neither of these approaches may not be good enough when dealing with worn shape of rails and wheels where a non-Hertzian contact occurs. The CONTACT algorithm is more suitable for these problems. Therefore a model created to study effects of the shape irregularities as well as the method of contact force estimation is presented in this paper.

2. Railway vehicle movement model

Railway vehicle is a complex system, therefore its model has to be simplified with respect to goal of the study. This study is focused on calculation of contact force distribution, thus the most important part of the model is the model of contact forces and the shape irregularities are also taken into account. They also cause vibration, so models of vibration of the vehick and the track are present.

*Corresponding author. Tel.: +420 541142804, e-mail: radek.jandora@seznam.cz.

3. Track model

Track is modelled on three levels. The first level is the model of track geometry - curves, climbs and superelevation of the track have a great influence on dynamics of the vehicle and take effect on centrifugal forces and shifts in force distribution between the wheels. The second level is the model of track dynamics where rails are modelled as beams and sleepers and ballast as multibody system connected to the rails. This model is focused on vibrations caused by the vehicle and it is local because the vibrations are significant only about ten meters in front of and behind the vehicle. The third level of track model is the surface function which is used to calculate the contact forces and described in section 4.1.

3.1. Track geometry

Shape of the track in the global coordinate system is described by two functions. The first one is the function of the centreline of the unloaded track

$$\Gamma_k = \left[\; x_k(\lambda), \quad y_k(\lambda), \quad z_k(\lambda) \; \right]^T \tag{1}$$

where λ is distance from the beginning of the track. The track radius and gradient can be obtained using principles of differential geometry on this three-dimensional curve. The other function is the superelevation of the track $s_e(\lambda)$. Using these functions the local coordinate system can be created in such a way that its $x-\text{axis}$ coincides with the tangent of the track centreline and its $y-\text{axis}$ coincides with the superelevation of the track. The $z-\text{axis}$ completes right-handed coordinate system. Origin of this coordinate system is set to be on the track centreline and to put the vehicle centre of gravity in the $yz-\text{plane}$.

3.2. Model of track dynamics

Properties of the track regarding its behaviour during passage of a train including damping of vibrations caused by the train were investigated in many work thus far. Rails are modelled as elastic beams and sleepers and ballast are modelled as a multibody system shown on fig. 1. The ways to create a multibody system of the track is proposed in [9, 10]. Model used by the author was inspired by [1, 7]. However both studies differ in the way how rails are described. In [1] rails are modelled using finite elements as a solid body. On the other hand in [7] the analytical solution is used. In this model rails are discretized using a beam element (BEAM4 element of ANSYS as in [2]). However, all other properties of the model are the same as in [1]. The model is implemented in MATLAB to achieve best compatibility with other parts of the model.

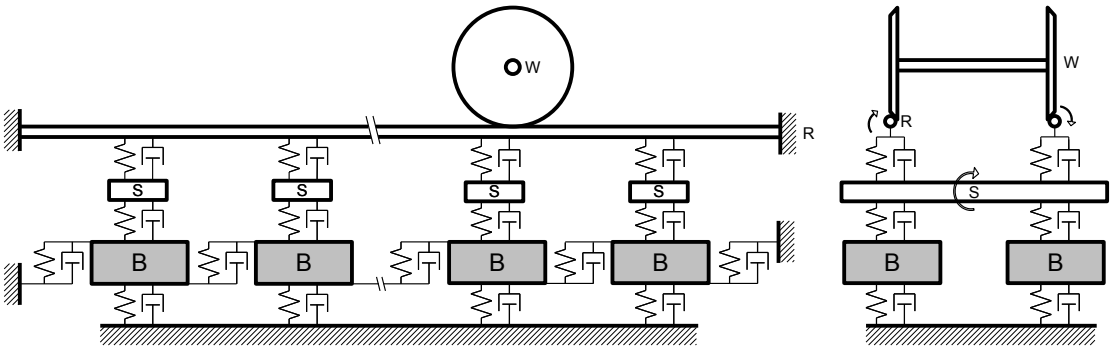

Fig. 1. The track model (B - ballast, S - sleeper, R - rail, W - wheelset).

Loads on the rails are obtained as the contact forces of the wheel-rail contact. These forces have an arbitrary position so they are divided into closest nodes. Then the system of differential equations is transformed into a state function which is input of the Runge-Kutta integration method in the way presented in [1].

4. Contact geometry

4.1. Rail corrugation and shape irregularities of wheel

Shape of each wheel is described in the wheelset cylindrical coordinate system (ρ_d, α_d, y_d) of the wheelset it belongs to. The $y_d-\mathrm{axis}$ coincides with the wheelset axis and the $\rho_d\alpha_d-\mathrm{plane}$ is normal to it. The origin of the coordinate system lies in the wheelset centre of gravity. In this coordinate system the shape is described with the function R which is the sum of the ideal wheel radius R_{id} (e.g. the S1002 profile) and the shape irregularities R_{irr}:

$$R\left(\alpha_d, y_d\right) = R_{id}\left(y_d\right) + R_{irr}\left(\alpha_d, y_d\right) \tag{2}$$

Shape of rails is described in the rail coordinate system (x_r, y_r, z_r). It is set accordingly to the position of the rail so its origin is placed in the immediate position of center of rail section and it is rotated to the same position as in the model of track dynamics. The rail surface function N is again sum of the ideal rail shape N_{id} (e.g. the UIC60 profile) and the corrugation N_{irr}:

$$N\left(x_r, y_r\right) = N_{id}\left(y_r\right) + N_{irr}\left(x_r, y_r\right) \tag{3}$$

4.2. Distance of the surfaces

The distance of the undeformed surfaces h is the key input for the estimation of the normal contact force. It can be expressed in two ways: as distance from a point of the wheel $h_w\left(\alpha_d, y_d\right)$ or as distance from a point of the rail $h_r\left(x_r, y_r\right)$.
When the distance is calculated, points of the both surfaces on the same line normal to one of the surfaces have to be obtained first as well as the orientation of the normal. The point of the rail $\mathbf{x}_r$ and the normal vector $\mathbf{n}_r$ are:

$$\mathbf{x}_r = \left[\begin{array}{ccc} x_r, & y_r, & N\left(x_r, y_r\right) \end{array}\right]^T \tag{4}$$

$$\mathbf{t}_{r,1} = \left[\begin{array}{ccc} 1, & 0, & \frac{\partial N}{\partial x_r} \end{array}\right]^T \qquad \mathbf{t}_{r,2} = \left[\begin{array}{ccc} 0, & 1, & \frac{\partial N}{\partial y_r} \end{array}\right]^T$$

$$\mathbf{n}_r = \frac{\mathbf{t}_{r,1} \times \mathbf{t}_{r,2}}{\left\|\mathbf{t}_{r,1} \times \mathbf{t}_{r,2}\right\|} \tag{5}$$

Similarly the point of the wheel $\mathbf{x}_w$ and the normal to the wheel $\mathbf{n}_w$ are:

$$\mathbf{x}_w = \mathbf{C}_{WR} \cdot \left[\begin{array}{c} R \cdot \cos\alpha_d \\ y_d \\ R \cdot \sin\alpha_d \end{array}\right] + \mathbf{x}_{wcg} \tag{6}$$

$$\mathbf{t}_{w,1} = \left[\begin{array}{ccc} \frac{dR}{d\alpha_d} \cdot \cos\alpha_d - R \cdot \sin\alpha_d, & 0, & \frac{dR}{d\alpha_d} \cdot \sin\alpha_d + R \cdot \cos\alpha_d \end{array}\right]^T$$

$$\mathbf{t}_{w,2} = \left[\begin{array}{ccc} \frac{dR}{dy_d} \cdot \cos\alpha_d, & 1, & \frac{dR}{dy_d} \cdot \sin\alpha_d \end{array}\right]^T$$

$$\mathbf{n}_w = \mathbf{C}_{WR} \cdot \frac{\mathbf{t}_{w,1} \times \mathbf{t}_{w,2}}{\left\|\mathbf{t}_{w,1} \times \mathbf{t}_{w,2}\right\|} \tag{7}$$

where $\mathbf{C}_{WR}$ is the matrix of transformation from the wheelset Cartesian coordinate system to the rail coordinate system and $\mathbf{x}_{wcg}$ is the position of the wheelset centre of gravity in the rail coordinate system. Corresponding points and their distance can be found using vector equation

$$0 = \mathbf{x}_r + h_r \cdot \mathbf{n}_r - \mathbf{x}_w \tag{8}$$

for a point of the rail or equation

$$0 = \mathbf{x}_r + h_w \cdot \mathbf{n}_w - \mathbf{x}_w \tag{9}$$

for the point of the wheel. Both equations make systems of three non-linear equations. The eq. 8 has to be solved as a three-dimensional problem because inverse function to $R(\alpha_d, y_d)$ cannot be found in most cases, thus point $\mathbf{x}_w(x_r, y_r)$ cannot be expressed explicitly. However, in the solution of the eq. 9 the problem can be reduced to one dimension:

$$\begin{aligned} x_r &= -h_w \cdot n_{w,1} + x_w(\alpha_d, y_d) \\ y_r &= -h_w \cdot n_{w,2} + y_w(\alpha_d, y_d) \\ 0 &= -h_w \cdot n_{w,3} + z_w(\alpha_d, y_d) - N(x_r, y_r) \end{aligned} \tag{10}$$

So the distances from the points of the wheel are easier to calculate, however the function is expressed in cylindrical coordinates so it does not provide actual shape of the gap/penetration of the surfaces. On the other hand the distances from the points of the rail are harder to get but they are an actual representation of the gap/penetration of the surfaces.

5. Contact forces

Next step is the calculation of the contact forces. Information required for the estimation of the normal force is the distance of the surfaces which was found in the previous step. For the tangential force the rolling velocity and relative velocities are required.
When solving the contact forces in the wheel rail contact, two different approaches can be used. It can be assumed that the contact patch is in the shape of ellipse or that the contact patch has an arbitrary shape.

5.1. Normal forces

5.1.1. Hertzian contact

Hertz theory of contact assumes that the contact patch is elliptic. The inputs of the algorithm are the normal of the surface and the minimum of the distance function which is found using the simplex method. It can be greater than zero (gap between the wheel and the rail) or less than zero (wheel and rail in contact and deformed). In the point of the extreme the centre of the contact ellipse is expected.
Undeformed distance of the surfaces in contact according to the Hertz theory of contact as presented in [8, 3] is in the form of

$$d_{cs} = D_{1,1} \cdot x^2 + D_{2,2} \cdot y^2 - h \tag{11}$$

where $D_{1,1}$ and $D_{2,2}$ are the principal curvatures of the contact pair. They can be calculated with the algorithm described in [4]. They are used to get excentricity m through the axial function

$$\left| \frac{D_{1,1} - D_{2,2}}{D_{1,1} + D_{2,2}} \right| = m^2 \cdot \frac{\mathbf{D}(m^2) - \mathbf{C}(m^2)}{\mathbf{E}(m^2)} \tag{12}$$

as shown in [8]. The size of the normal force is then

$$N = \frac{2 \cdot \pi \cdot G}{3 \cdot (1-\mu)} \cdot \sqrt{\frac{\mathbf{E} \cdot (-h)^3}{(D_{1,1} + D_{2,2}) \cdot k_e \cdot \mathbf{K}^3}} \tag{13}$$

and the half-axes of the contact ellipse are

$$k_e = \begin{cases} 1 - m^2 & \text{for} \quad D_{1,1} \leq D_{2,2} \\ \frac{1}{1-m^2} & \text{for} \quad D_{1,1} > D_{2,2} \end{cases} \tag{14}$$

$$a_{ce} = \sqrt[3]{\frac{3 \cdot N \cdot (1-\mu) \cdot \mathbf{E}}{2 \cdot \pi \cdot G\,(D_{1,1} + D_{2,2}) \cdot k_e}} \tag{15}$$

$$b_{ce} = a_{ce} \cdot \sqrt{k_e} \tag{16}$$

G is the modulus of rigidity and μ is the Poissons ratio, $\mathbf{C}$, $\mathbf{D}$, $\mathbf{E}$, $\mathbf{K}$ are complete elliptic integrals, k_e is ratio of squares of half-axes. The normal force is then

$$\mathbf{N} = N \cdot \mathbf{n}_w \tag{17}$$

5.1.2. NORM algorithm

The NORM algorithm is the first step of the CONTACT algorithm created by Kalker (described in [8] and [3]). It is a method based on boundary element method and methods of nonlinear optimization. The expected contact area is discretized and the influence matrix accordingly to the representation of Boussinesq and Cerruti (as presented in [8]) is calculated for each element. The original NORM algorithm was created on assumption of elastic half-space. However, when arbitrary geometry is used, this supposition is no longer valid. To compansate this a complementary principle for arbitrary geometry was derived in [6]. According to this principle a new version was created. Now the input of the algorithm is not only the distance of the contact surfaces but also the normal of the rail surface for each element. Because the surface is curved now, the assumption of the elastic half-space does not hold. However, the deformation of the influence area is considered very small compared to the size of the wheel or the rail. Therefore the assumption of the elastic half-space is kept with supposition that results are still accurate enough. Then the normal tractions are found when the system of equations

$$e_I = h_I + A_{I3Jj} \cdot p_{Jj} \tag{18}$$

$e_I = 0$ if element I lies inside the contact patch
$p_{Jj} = 0$ if element I lies outside the contact patch

is solved and all elements are correctly placed into or out of the contact patch. e_I is the deformed distance, h_I is the undeformed distance, A_{IiJj} is the influence matrix and p_{Jj} is the load on the surface. Normal force is calculated as

$$\mathbf{N} = \sum_I p_{I3} \cdot \mathbf{n}_{r,I} \cdot dS_I \tag{19}$$

5.2. Tangential forces

Tangential forces depend on the velocity of the vehicle, on relative velocities in the contact patch, on the normal forces and on the coefficient of adhesion. The velocity of the wheelset centre of gravity can be considered the rolling velocity

$$\mathbf{v}_{rol} = \|\mathbf{x}_{wcg}\| \tag{20}$$

and its magnitude is labelled V. They are important inputs into the algorithms of the tangential force calculation. The algorithms created for the elliptic contact patch require projection of the rolling velocity into the principal coordinate system of the contact ellipse:

$$\mathbf{v}_{rol,CP} = \begin{bmatrix} 1 & 0 & 0 \\ 0 & 1 & 0 \\ 0 & 0 & 0 \end{bmatrix} \cdot \mathbf{C}_{CP}^{T} \cdot \dot{\mathbf{x}}_{wcg} \tag{21}$$

$\mathbf{C}_{CP}$ is the transformation matrix of the principal coordinate system of the contact ellipse which is found with principal curvatures $D_{1,1}$ and $D_{2,2}$ used in eq. 11 and it is obtained by the algorithm described in [4].
Rolling contact theories assume the $x-$axis of the contact patch is identical with the direction of the rolling velocity; therefore the coordinate system of the contact patch has to be once again rotated about the angle ε_{rol}

$$\mathbf{C}_{rol} = \begin{bmatrix} \cos\varepsilon_{rol} & -\sin\varepsilon_{rol} & 0 \\ \sin\varepsilon_{rol} & \cos\varepsilon_{rol} & 0 \\ 0 & 0 & 1 \end{bmatrix} \tag{22}$$

The velocity of the point of the wheel in the coordinate system of the rolling velocity is

$$\mathbf{v}_c = \mathbf{C}_{rol}^{T} \cdot \mathbf{C}_{CP}^{T} \cdot \left(\mathbf{\Omega}_{WR} \cdot \mathbf{C}_{WR} \cdot \begin{bmatrix} R \cdot \cos\alpha_d \\ y_d \\ R \cdot \sin\alpha_d \end{bmatrix} + \dot{\mathbf{x}}_{wcg} \right) \tag{23}$$

where $\mathbf{\Omega}_{WR}$ is the matrix of the angular velocity of the wheelset and it can be rewritten into the form of vector ω_{WR}. Angular velocity of the wheelset is:

$$\omega_c = \mathbf{C}_{rol}^{T} \cdot \mathbf{C}_{CP}^{T} \cdot \omega_{WR} \tag{24}$$

The coordinate system is bound to the rail so these values are the rigid slip and the rigid spin in the contact patch. Values of the longitudinal creepage υ_x, lateral creepage υ_y and spin creepage ϕ_z are

$$\upsilon_x = \frac{v_{c,1}}{V} \tag{25}$$

$$\upsilon_y = \frac{v_{c,2}}{V} \tag{26}$$

$$\phi_z = \frac{\omega_{c,3}}{V} \tag{27}$$

Now the contact forces can be calculated.

5.2.1. Kalker's linear theory of rolling contact

The linear theory of rolling contact in [8] assumes adhesion in the whole contact patch. The tangential forces and the spin moment have linear dependence on the creepages

$$T_x = -G \cdot a_{ce} \cdot b_{ce} \cdot C_{11} \cdot \upsilon_x \tag{28}$$

$$T_y = -G \cdot a_{ce} \cdot b_{ce} \cdot C_{22} \cdot \upsilon_y - G \cdot (a_{ce} \cdot b_{ce})^{\frac{3}{2}} \cdot C_{23} \cdot \phi_z \tag{29}$$

$$M_z = -G \cdot (a_{ce} \cdot b_{ce})^{\frac{3}{2}} \cdot C_{32} \cdot \upsilon_y - G \cdot (a_{ce} \cdot b_{ce})^{2} \cdot C_{33} \cdot \phi_z \tag{30}$$

Here C_{11}, C_{22}, $C_{23} = -C_{32}$ and C_{33} are Kalker's creepage coefficients which are functions of half-axes of the contact ellipse a_{ce} and b_{ce} obtained in eq. 15 and 16. They are calculated numerically and tabulated in [8].

5.2.2. Vermeulen & Johnson theory

While the contact forces are linearly dependent on creepages in the previous step, in reality they saturate on value

$$T = f \cdot N \tag{31}$$

where f is the coefficient of adhesion. Therefore accordingly to the Vermeulen & Johnson theory as presented in [8] the tangential forces calculated by the linear theory are modified by the following function:

$$T = \sqrt{T_x^2 + T_y^2} \tag{32}$$

$$w' = \frac{T}{3 \cdot f \cdot N} \tag{33}$$

$$\bar{T} = \begin{cases} f \cdot N \cdot \left[1 - (1 - w')^2\right] & \text{pro} \quad w' \leq 1 \\ f \cdot N & \text{pro} \quad w' > 1 \end{cases} \tag{34}$$

$$\bar{T}_x = \frac{T_x}{T}\bar{T} \tag{35}$$

$$T_y = \frac{T_y}{T}\bar{T} \tag{36}$$

Now slip is taken into account. However, the Vermeulen & Johnson theory is applicable only when spin is zero or insignificant.

5.2.3. FASTSIM algorithm

The FASTSIM algorithm (in [8], [3]) has to be applied in order to calculate the contact forces when spin is significant. Then the contact area is discretized and the simplified theory of contact is used. In the simplified theory the bodies in contact are replaced by a set of springs capable of bending. Their bending stiffness can be calculated

$$L = \frac{\frac{8 \cdot a_{ce}}{3 \cdot G \cdot C_{11}} \cdot |v_x| + \frac{8 \cdot a_{ce}}{3 \cdot G \cdot C_{22}} \cdot |v_y| + \frac{\pi \cdot a_{ce}^2}{4 \cdot G \cdot C_{23} \cdot \sqrt{a_{ce} \cdot b_{ce}}} \cdot |\phi_z| \cdot \sqrt{a_{ce} \cdot b_{ce}}}{\sqrt{v_x^2 + v_y^2 + a_{ce} \cdot b_{ce} \cdot \phi_z^2}} \tag{37}$$

Rigid slip of an element is

$$c_{I,1} = (v_x - y_I \cdot \phi_z) \cdot V \tag{38}$$

$$c_{I,2} = (v_y - x_I \cdot \phi_z) \cdot V \tag{39}$$

Then in the adhesion area the tangential tractions are

$$p_{I\tau}^H(t) = p_{I\tau} \cdot (t - dt) - \frac{dt}{L} \cdot c_{I\tau} \tag{40}$$

In the slip area

$$p_{I\tau}^S = f \cdot \frac{2 \cdot N}{\pi \cdot a_{ce} \cdot b_{ce}} \cdot \left(1 - \frac{x_I^2}{a_{ce}^2} - \frac{y_I^2}{b_{ce}^2}\right) \cdot \frac{p_{I\tau}^H}{\|p_{I\tau}^H\|} \tag{41}$$

$$s_{I\tau} = c_{I\tau} + \frac{L}{dt} \cdot \left[p_{I\tau}^S(t) - p_{I\tau}(t - dt)\right] \tag{42}$$

The contact forces are

$$T_x = \sum_I p_{I,1} dS \tag{43}$$

$$T_y = \sum_I p_{I,2} dS \tag{44}$$

$$M_z = \sum_I \left(x_I \cdot p_{I,2} - y_I \cdot p_{I,1}\right) dS \tag{45}$$

5.2.4. TANG algorithm

The TANG algorithm (in [8], [3]) succeeds to the NORM algorithm. Its principles are similar. For the same elements the influence matrices A_{IiJj} (current influence) and B_{IiJj} (influence of the previous time step) are created. The input of the TANG algorithm is the rigid slip $c_{I\tau}$ of each element of the contact patch. This rigid slip is the relative velocity of the element

$$c_{I\tau} = v_{c,I\tau}\left(x_r, y_r\right) \tag{46}$$

Then system of equations

$$s_{I\tau} = c_{I\tau} + \frac{A_{I\tau Jj} \cdot p_{Jj}\left(t\right) - B_{I\tau Jj} \cdot p_{Jj}\left(t - dt\right)}{dt} \tag{47}$$

$s_{I\tau} = 0$ if element is in the adhesion area
$s_{I\tau} = -S_I \cdot \frac{p_{I\tau}}{f p_{I3}}$ and $p_{I1}^2 + p_{I2}^2 = f^2 p_{I3}^2$ if element is in the slip area

is solved and all elements are placed into the right area. Then tangential force is

$$\mathbf{T} = \sum_{I,\tau} p_{I\tau} \cdot \mathbf{t}_{r,I\tau} \cdot dS_I \tag{48}$$

where $\mathbf{t}_{r,I\tau}$ are the tangential axes of the element surface.

5.3. Transformation of the contact forces

The contact forces calculated with each method are placed in the coordinate system the algorithm used. Therefore they have to be placed into the global coordinate system to study the vehicle motion.

6. Vehicle motion

The railway vehicle can be modelled as a multibody system of the vehicle body (fig. 2), the bogies and the wheelsets and the connecting elements - springs and dampers. Thus motion of each of the bodies is ruled by its inertia, gravity and forces applied on it.

6.1. Wheelset motion

The wheelsets are in contact with the rail so the contact forces are applied on them. The wheelset are connected to the bogie, therefore springs and dampers connecting the wheelset and

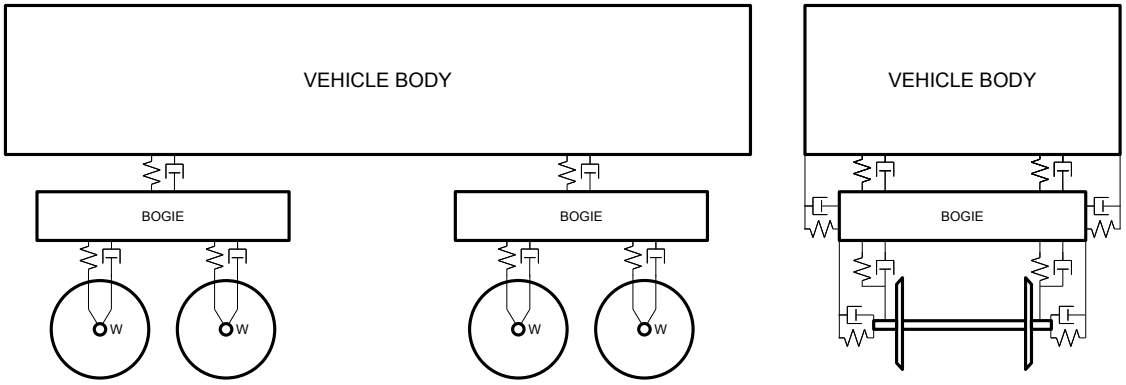

Fig. 2. The vehicle model (W - wheelset).

the bogie influence the wheelset. Then equations of motion are

$$\ddot{\mathbf{x}}_{wcg} = \frac{1}{m_w} \cdot \left(\mathbf{F}^L_{con} + \mathbf{F}^R_{con} + \sum_k \mathbf{F}_{BW,k} \right) + \mathbf{g} \tag{49}$$

$$\begin{aligned} \alpha_w &= \mathbf{J}_w^{-1} \cdot \Big[\left(\mathbf{x}^L_{con} - \mathbf{x}_{wcg} \right) \times \mathbf{F}^L_{con} + \left(\mathbf{x}^R_{con} - \mathbf{x}_{wcg} \right) \times \mathbf{F}^R_{con} + \mathbf{M}^L_{con} + \mathbf{M}^R_{con} + \\ &+ \sum_k \left(\mathbf{x}_{BW,k} - \mathbf{x}_{wcg} \right) \times \mathbf{F}_{BW,k} + \sum_k \mathbf{M}_{BW,k} \Big] \end{aligned} \tag{50}$$

where $\mathbf{F}^L_{con}$, $\mathbf{F}^R_{con}$, $\mathbf{M}^L_{con}$ and $\mathbf{M}^R_{con}$ are the contact forces and moments, $\mathbf{x}^L_{con}$ and $\mathbf{x}^R_{con}$ positions of the contact patches; $\mathbf{F}_{BW,k}$ and $\mathbf{M}_{BW,k}$ are the forces and moments by springs and dampers connecting the wheelset to the bogie and $\mathbf{x}_{BW,k}$ positions of that forces; m_w is the mass of the wheelset, $\mathbf{J}_w$ is the matrix of the moment of inertia of the wheelset; $\ddot{\mathbf{x}}_{wcg}$ acceleration of the wheelset translation movement and α_w angular acceleration of the wheelset rotation.

6.2. Bogie motion

The bogie is connected to the wheelsets and to the vehicle body, thus its motion is influenced by the elements connecting it to them:

$$\ddot{\mathbf{x}}_{bcg} = \frac{1}{m_b} \cdot \left(\sum_k \mathbf{F}_{VB,k} + \sum_k \mathbf{F}_{BW,k} \right) + \mathbf{g} \tag{51}$$

$$\begin{aligned} \alpha_b &= \mathbf{J}_b^{-1} \cdot \left[\sum_k \left(\mathbf{x}_{VB,k} - \mathbf{x}_{bcg} \right) \times \mathbf{F}_{VB,k} + \sum_k \mathbf{M}_{VB,k} + \right. \\ &+ \left. \sum_k \left(\mathbf{x}_{BW,k} - \mathbf{x}_{bcg} \right) \times \mathbf{F}_{BW,k} + \sum_k \mathbf{M}_{BW,k} \right] \end{aligned} \tag{52}$$

where $\mathbf{F}_{VB,k}$ and $\mathbf{M}_{VB,k}$ are the forces and moments by springs and dampers connecting the bogie to the vehicle body and $\mathbf{x}_{VB,k}$ positions of that forces; m_b is the mass of the bogie, $\mathbf{J}_b$ is the matrix of the moment of inertia of the bogie; $\ddot{\mathbf{x}}_{bcg}$ acceleration of the bogie translation movement and α_b angular acceleration of the bogie rotation.

6.3. Vehicle body motion

The vehicle body motion is influenced by the connected bogies and aerodynamic resistance:

$$\ddot{\mathbf{x}}_{vcg} = \frac{1}{m_v} \cdot \left(\sum_k \mathbf{F}_{VB,k} \mathbf{F}_{AR} \right) + \mathbf{g} \tag{53}$$

$$\alpha_v = \mathbf{J}_v^{-1} \cdot \left[\sum_k (\mathbf{x}_{VB,k} - \mathbf{x}_{vcg}) \times \mathbf{F}_{VB,k} + \sum_k \mathbf{M}_{VB,k} + \right] \tag{54}$$

where $\mathbf{F}_{AR}$ is the forces caused by aerodynamic resistance; m_v is the mass of the vehicle body, $\mathbf{J}_v$ is the matrix of the moment of inertia of the vehicle body; $\ddot{\mathbf{x}}_{vcg}$ acceleration of the vehicle body translation movement and α_v angular acceleration of the vehicle body rotation.

7. Conclusion

This model can be used to study many phenomenons which may happen in the railway travel. Its main usage is the estimation of the contact forces or contact pressure for the wear prediction. But it can be also used to simulate vibrations in the system and events that are very undesirable like derailments.

The most important part of the model is however the wheel-rail contact. In this model an arbitrary geometry of the contact forces is expected so it can be used to simulate both rail corrugation and irregularities of the shape of the wheels and dynamic effects they have on the system. With further finite element analyses wear prediction, fatigue or material, initiation and growth of cracks.

References

[1] C. Andersson, A. Johansson, Prediction of rail corrugation generated by three dimensional wheel-rail interaction, Wear 257 (2004) 423-434.

[2] ANSYS Theory Reference Manual, 14.4 BEAM4 - 3-D Elastic Beam, 2005.

[3] B. Jacobson, J.J. Kalker, Rolling Contact Phenomena, Springer-Verlag, 2000.

[4] R. Jandora, Modelling of the railway wheelset movement considering real geometry, Proc. of the Engineering Mechanics 2007 Conference in Svratka, Czech Republic.

[5] R. Jandora, A comparison of methods used to calculate contact forces, submitted to Dynamics of solid and elastic bodies 2007 Conference in Ústí n. L., Czech Republic.

[6] X.S. Jin, J.Y. Zhang, A complementary principle of elastic bodies of arbitrary geometry in rolling contact, Computers and Structures 79 (2001) 2635-2644.

[7] X.S. Jin, Z.F. Wen, K.Y. Wang, Z.R. Zhou, Q.Y. Liu, C.H. Li, Three-dimensional train-track model for study of rail corrugation, Journal of Sound and Vibration 293 (2006) 830-855.

[8] J.J. Kalker, Three Dimensional Elastic Bodies in Rolling Contact, Kluwer Academic Publishers, 1990.

[9] K. Knothe, Receptance behaviour of railway track and subgrade, Archive of Applied Mechanics 68 (1998) 457-470.

[10] H. Kruse, K. Popp, A modular algorithm for linear, periodic train-track models, Archive of Applied Mechanics 71 (2001) 473-786.